



Trans. Nonferrous Met. Soc. China 33(2023) 728-742

Transactions of **Nonferrous Metals** Society of China

www.tnmsc.cn



Microstructure evolution and deformation mechanism of Mg-Zn-Gd sheet during Erichsen cupping test

Yong CHEN^{1,2}, Hong YAN^{1,3}, Dan WANG⁴, Rong-shi CHEN^{1,2}

1. Shi-changxu Innovation Center for Advanced Materials, Institute of Metal Research, Chinese Academy of Sciences, Shenyang 110016, China;

2. School of Materials Science and Engineering,

University of Science and Technology of China, Shenyang 110016, China; 3. School of Materials Science and Engineering,

Shandong University of Science and Technology, Qingdao 266590, China;

4. AECC Shenyang Liming Aero-Engine Co., Ltd., Shenyang 110043, China

Received 15 November 2021; accepted 14 March 2022

Abstract: An Erichsen cupping test of GZ31 sheet at room temperature with different reductions was carried out, and four samples with IEs (Erichsen index) of 2.0, 4.1, 7.1, and 7.3 mm were obtained. The deformation and fracture mechanisms of the cupping deformation process were studied by OM, SEM and EBSD. The results show that the IE of the GZ31 rolled sheet with the non-basal texture can reach 7.3 mm. Basal and pyramidal dislocation slips and {1012} extension twinning are the main deformation modes during the Erichsen cupping test. The dislocation slip is hindered by the second phase particles and grain boundaries and entangles with each other to form voids, which eventually leads to the fracture of the material. The reason for the GZ31 sheet showing high IE is that the weak non-basal texture and rare earth elements are favorable for dislocation slip and extension twining to coordinate deformation.

Key words: magnesium alloy; Erichsen cupping test; dislocation slip; twining

1 Introduction

Compared with the cast magnesium alloys, wrought magnesium alloys usually have higher strength and better plasticity, and magnesium alloys in the form of sheets can be processed into various complex shapes by secondary forming techniques [1-5]. If magnesium alloy sheets are used to produce electronic shells through secondary forming technique at room temperature, the production efficiency and product quality will be greatly improved, and the cost will be reduced.

However, the existing commercial magnesium alloy sheets have a basal texture and thus poor rollability formability at room temperature [6–8]. For example, a rolled AZ31 sheet usually forms a strong basal texture with a texture peak intensity of 6-10, and the elongation is approximately 20% at room temperature [9–11]. Erichsen cupping tests on rolled AZ31 magnesium alloy sheet suggested that the maximum IE was only 2-3.7 mm, which was only 1/3 that of commercial aluminum alloy 6061 [12,13]. This means that AZ31 sheet generally has poor cupping performance and cannot be formed at room temperature.

Recent research results show that the addition of rare earth elements to magnesium alloys can effectively regulate the texture, and significantly improve the rolled sheet ductility and secondary formability [14,15]. YAN et al [16] found that the Mg-Zn-RE alloy formed a weak double-peak non-basal texture after hot rolling. The orientation distribution is wider in transverse direction (TD) than in rolling direction (RD), and the peak intensity is only approximately half that of AZ31. The IEs of Mg-1.5Zn-0.2%Y/Ce/Gd alloys are 4.9, 5.8 and 7.0 mm, respectively, which are much higher than those of the AZ31 sheet [17]. Among them, the Mg-Zn-Gd alloy has the best formability because of higher solid solubility of Gd and less second phase in the microstructure.

Although researchers have studied the uniaxial tension-compression deformation mechanism of the Mg-Zn-RE sheet, the deformation behavior during secondary forming has seldom been investigated. addition, strain/stress the circumstances more complicated are during secondary forming than during uniaxial deformation.

The Erichsen cupping test [18] is the oldest and most popular test in the sheet formability test. Therefore, in this study, the microstructure evolution and macroscopic cracks of an annealed Mg-1Zn-3Gd sheet were observed during the Erichsen cupping test. Base on this, the plastic deformation mechanism and fracture mechanism were studied, aiming to analyze the reason for the improvement in room-temperature formability. This study provides an experimental basis for the optimization of the deformation process and promotes industrial application of high-ductility magnesium alloys.

2 Experimental

An annealed Mg-3Gd-1Zn (referred to as GZ31) magnesium alloy sheet was used for the Erichsen cupping test, and the chemical composition was Mg-2.61Gd-1.03Zn (wt.%).

The cupping test was carried out following GB/T 4156—2007 (Metallic materials—Sheet and strip—Erichsen cupping test). The equipment used was a PS2705 cupping tester, the standard punch size was $d(20\pm0.5)$ mm, and the punching speed was 1 mm/min. The schematic diagram of the Erichsen cupping test in this study is shown in Fig. 1. The principle of the experiment is as follows: a punch with a spherical end was used to punch the metal sheet sample clamped between the die and the cushion die. During the test, the sheet was pushed into a hemispherical bulge by the punch until the

sample showed a light-transmitting crack. The IE of the annealed Mg–Zn–Gd was measured to be 7.3 mm. To study the microstructure during the Erichsen cupping test, another four cupping tests were performed and interrupted at punch depths of 2.0, 4.1, and 7.1 mm, respectively.

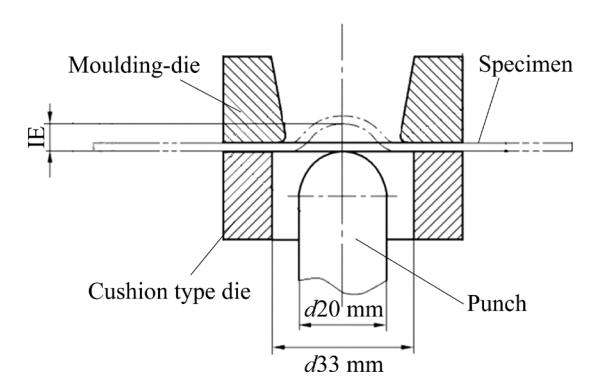


Fig. 1 Schematic diagram of Erichsen cupping test

The samples for microstructure observation were cut via wire electrical discharge machining on the cupped samples, and the sampling position is shown in Fig. 2. The white square in Fig. 2(a) is the sampling position of the metallographic sample, and the white square in Fig. 2(b) is the position for EBSD analysis. The observation surface is the RD-TD plane, and the sample size is 8 mm (RD) × 5 mm (TD). The microstructure of the samples was observed on a Zeiss optical microscope (OM) and scanning electron microscope (SEM, Philips XL30 ESEM-FEG/EDAX). The etching solution was 25 mL ethanol + 2 g picric acid + 5 mL acetic acid + 5 mL water. The surface macro-texture of the sheet (RD-TD plane) was analyzed by a Bruker D8 X-ray diffractometer, using single Cu K_α radiation with a measurement angle of 0° -70°. The texture data were corrected with magnesium powder and processed by DIFFRACplus TEXEVAl software. After mechanical and electrochemical (10 vol.% perchloric acid and 90 vol.% ethanol electrolyte) polishing, electron backscattered diffraction (EBSD) measurement of the samples was carried out on a HITACHI SE3400N SEM equipped with an HKL-EBSD system. The scanning step size was 0.6 µm, the operating voltage was 20.0 kV, and the analysis software was AztecCrystal. Tensile tests were conducted at room temperature with an initial train rate of 1×10⁻³ s⁻¹ on a universal testing machine. The dimensions of tensile test sample are shown in Fig. 3.

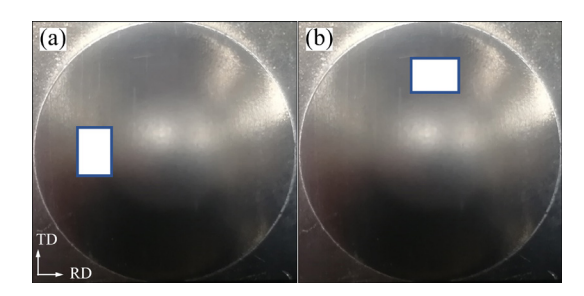


Fig. 2 Sampling locations for different tests: (a) OM and SEM; (b) EBSD

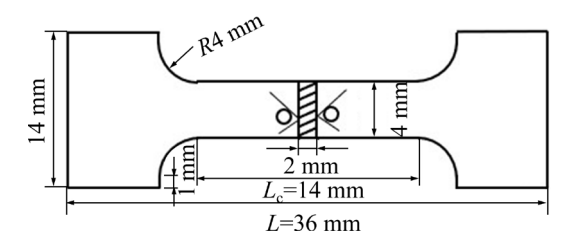


Fig. 3 Dimensions of tensile test samples

3 Results and discussion

3.1 Microstructure, texture and mechanical properties of annealed sheet

The microstructure of the GZ31 sheet annealed at 350 °C for 2 h is shown in Fig. 4(a). It has relatively uniform equiaxed grain microstructure with an average grain size of 39.32 µm measured by the linear intercept method. As can be seen from Fig. 4(b), there are a large number of fine and dispersed second phases in the matrix. According to the reported literature [19], we know that they are the Mg₅Gd binary phase and Mg₃Gd₂Zn₃ ternary phase. Figure 5 shows the macro-texture of the annealed sheet. It can be seen that the texture is the typical non-basal texture with two TD-split texture components tilting away from the normal direction (ND) to the TD by $\sim 50^{\circ}$. The texture intensity is 2.2, which is significantly lower than that (8.4) of AZ31 sheet [20]. Table 1 shows the tensile properties of the annealed GZ31 sheet at room temperature. The elongations along the RD and TD are both approximately 23%, and the strengths are similar, indicating that the anisotropy is not obvious.

3.2 Macroscopic morphology and microstructure of cupped samples

The top and side morphologies of the samples with IEs of 2.0, 4.1, 7.1, and 7.3 mm are shown in

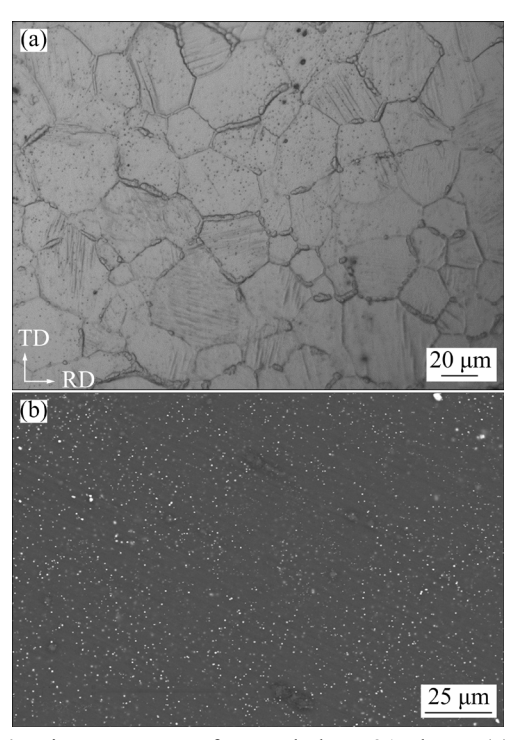


Fig. 4 Microstructure of annealed GZ31 sheet: (a) OM image; (b) SEM image

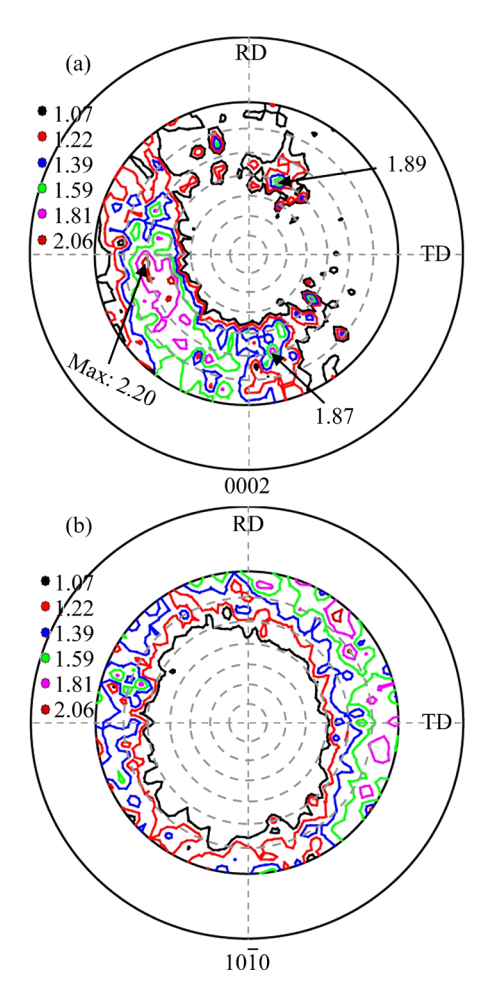


Fig. 5 Pole figures of annealed GZ31 sheet: (a) (0002); (b) $(10\overline{10})$

Table 1 Tensile mechanical properties of annealed GZ31 sheet at room temperature

| Direction | YS/MPa | UTS/MPa | EL/% |
|-----------|--------|---------|--------|
| RD | 83±3 | 196±2 | 22±1 |
| TD | 80±2 | 188±5 | 25.5±1 |
| 45° | 90±2.5 | 191±3 | 30±4 |

YS: Yield strength; UTS: Ultimate tensile strength; EL: Elongation to failure

Fig. 6. We can see that the samples with IEs of 2.0, 4.1, and 7.1 mm do not show any cracks, and the cupped sample with IE of 7.3 mm produced crack along the TD. According to the judging standard of

the Erichsen cupping test, the IE of the annealed GZ31 sheet can reach 7.3 mm. From the perspective of surface roughness, the surfaces of the cupped samples with IEs of 7.1 and 7.3 mm are significantly smoother than those of the samples with IEs of 4.1 and 2.0 mm, indicating that the amount of deformation is greater and obvious plastic deformation has occurred.

Figures 7(a) and (b) show the OM and EBSD images of the samples with different IEs, respectively. It can be seen that the microstructures are relatively uniform equiaxed crystals. The grain sizes of samples with IEs of 0, 4.1 and 7.1 mm were calculated as

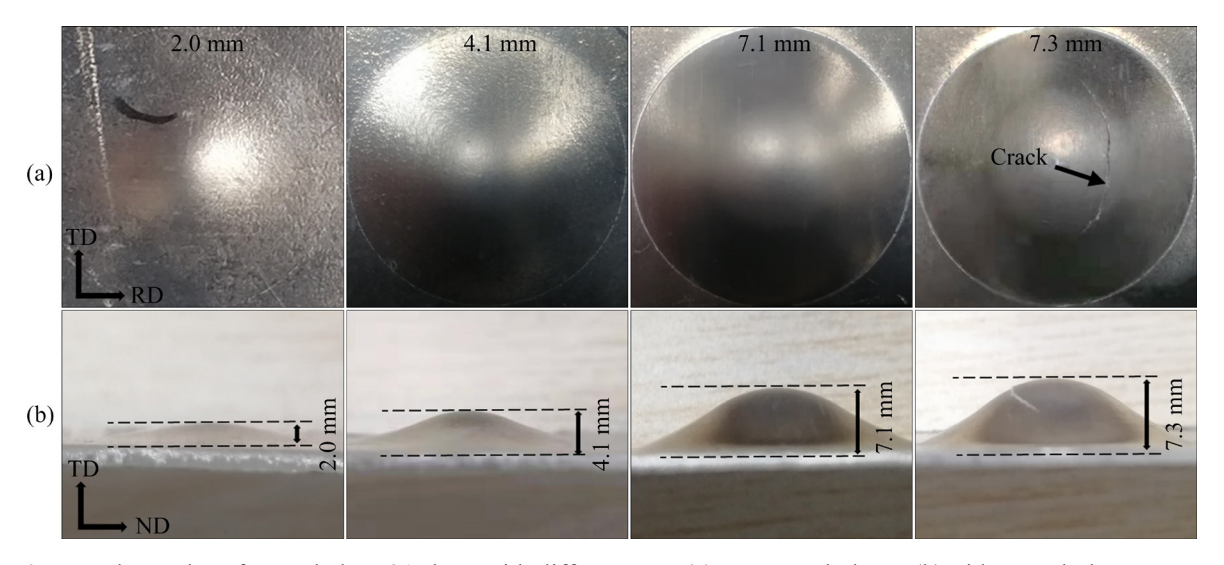


Fig. 6 Cupped samples of annealed GZ31 sheet with different IEs: (a) Top morphology; (b) Side morphology

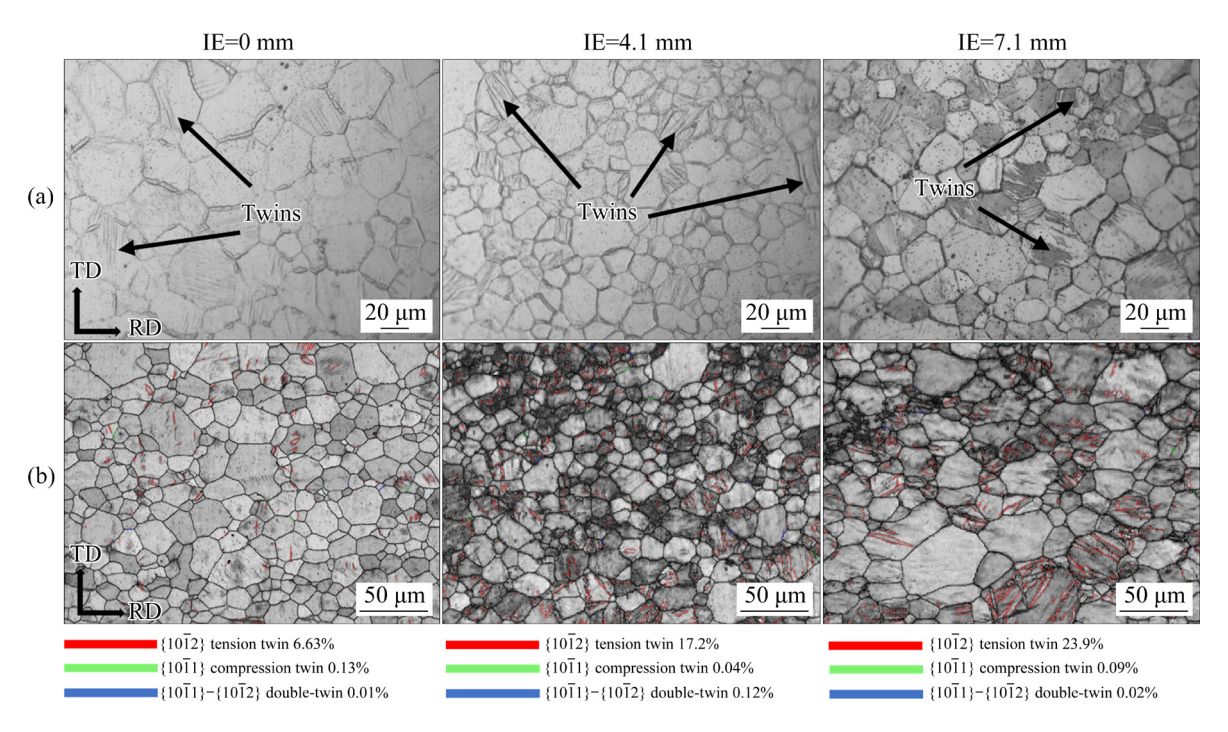


Fig. 7 Microstructures of cupped samples with different IEs: (a) OM image; (b) EBSD image

39.32, 42.58 and 49.58 μ m, respectively. This shows that the grain sizes increase with increasing deformation. A few twins can be seen, and they are identified as $\{10\,\overline{1}2\}$ extension twins after EBSD analysis. With the increase of IE, the number fraction of $\{10\,\overline{1}2\}$ extension twins increased continuously, which were 6.63%, 17.2% and 23.9%, respectively. Compared those with IEs of 7.1 and 4.1 mm, the $\{10\,\overline{1}2\}$ extension twins of the sample with IE=7.1 mm are wider, indicating that the $\{10\,\overline{1}2\}$ extension twins grow with the increasing deformation. It is inferred that the $\{10\,\overline{1}2\}$ extension twining plays a certain role during the cupping deformation.

Figure 8 shows the microstructures of the sample at different positions with IE=7.1 mm. Figure 8(a) shows the schematic diagram of the sampling location and the thickness size of the cupped sample. Figures 8(b-e) show the OM images at Positions 1, 2, 3 and 4, respectively. It can be

seen from Fig. 8(a) that the degree of deformation at different positions is different, and the thicknesses at Positions 1, 2, 3 and 4 are 890, 865, 767 and 776 μ m, respectively. Among them, the thickness of Position 3 is the smallest. This position is the place where macro-cracks are generated. Twins are observed in all different microstructures, and the microstructures at Positions 3 and 4 have greater roughness and seem to contain more defects because of the larger strain.

3.3 Deformation mechanism

To analyze the deformation mechanism during the Erichsen cupping test, samples with IEs of 0, 4.1 and 7.1 mm were selected for EBSD analysis, as shown in Fig. 9. The inverse pole figures (IPF) of Figs. 9(a, b, c) mark the misorientation between some twins and the matrix. These angles are all approximately 86°, which indicates that these twins

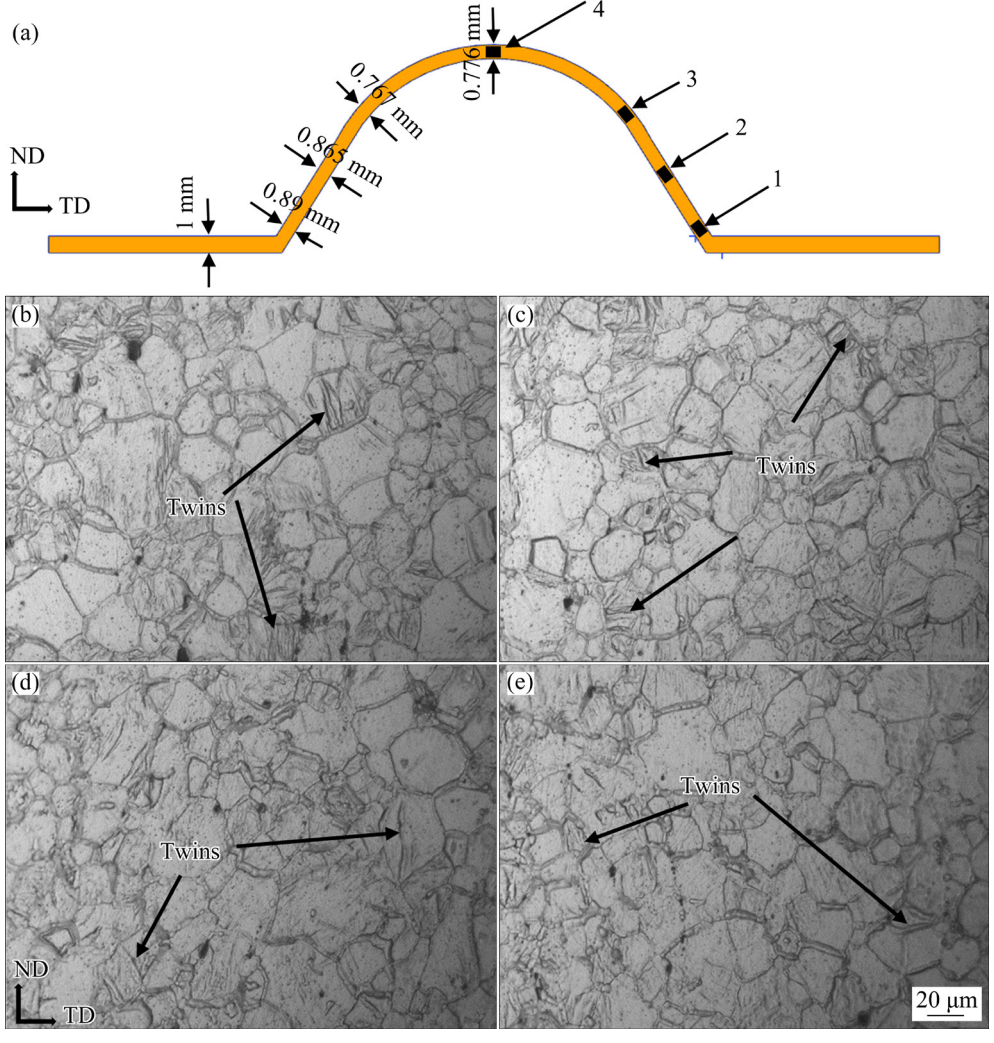


Fig. 8 Microstructures of sample with IE of 7.1 mm: (a) Schematic diagram of OM sampling position; (b-e) Microstructures at Positions 1, 2, 3 and 4, respectively

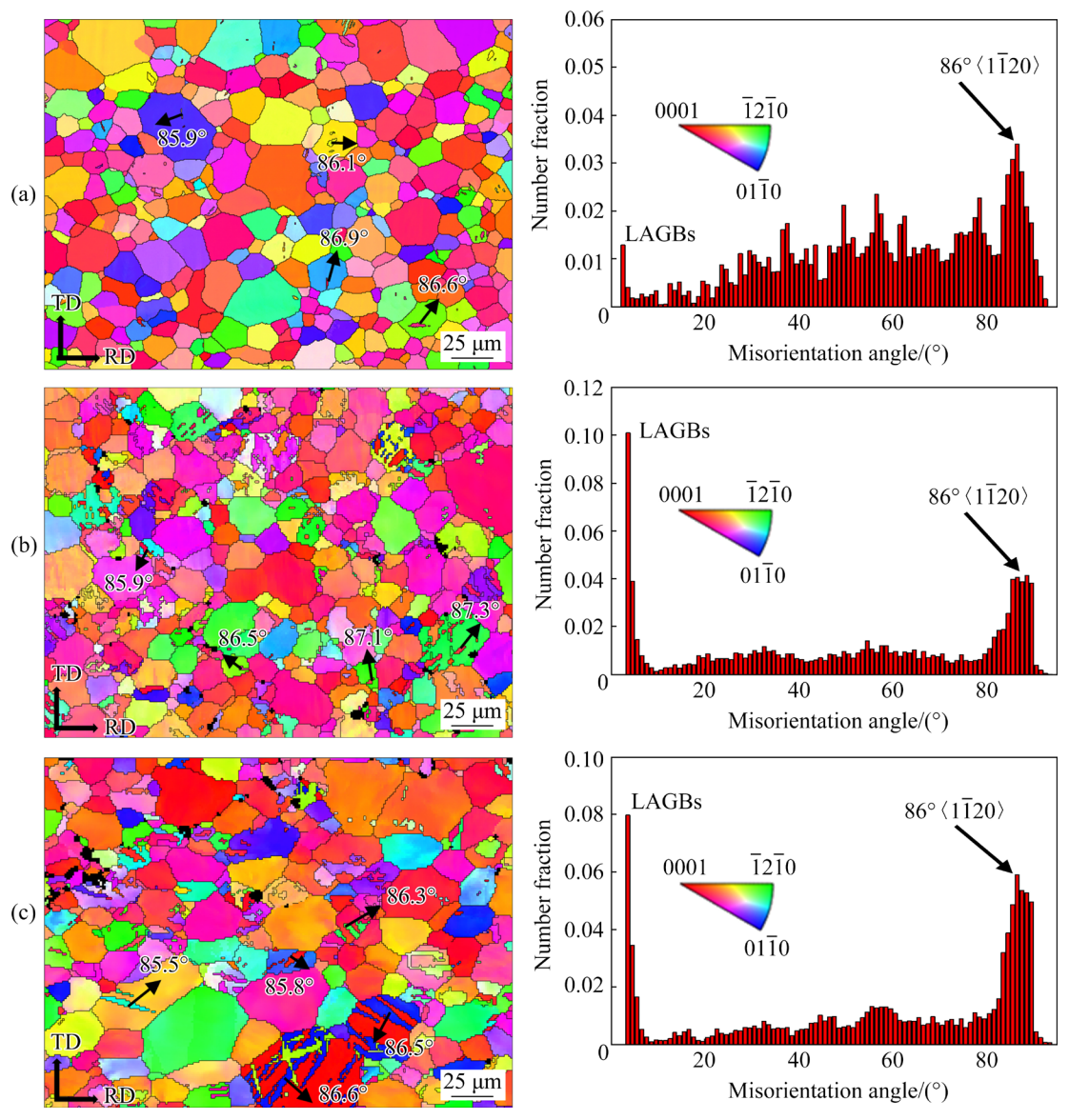


Fig. 9 Grain boundary misorientation analysis results of samples with different IEs: (a) IE=0 mm; (b) IE=4.1 mm; (c) IE=7.1 mm

are $\{10\overline{12}\}$ extension twins. The peak values of the misorientation angle distribution appear at $2^{\circ}-6^{\circ}$ and 86° , corresponding to the low angle grain boundaries (LAGBs) and the extension twining boundary, respectively. Generally, LAGBs are mostly caused by the dislocation slip accumulation [21], so, it is concluded that dislocation slip and $\{10\overline{12}\}$ extension twinning are the main deformation modes during the Erichsen cupping test process.

By comparing Fig. 9(a) with Fig. 9(b), it can be found that the number fraction of {1012} extension twins slightly increases with increasing IE, while the number of LAGBs increases significantly. Therefore, it can be inferred that

dislocation slip is the dominant factor during the deformation process from IE=0 mm to IE=4.1 mm. By comparing Fig. 9(b) with Fig. 9(c), it can be seen that LAGBs are slightly reduced, while the number fraction of the {1012} extension twin boundary has increased. Based on this, it is speculated that the {1012} extension twining initiates coordinated deformation during the deformation process from IE=4.1 mm to IE=7.1 mm.

Figure 10 shows the (0001) pole figures of IE=0, 4.1, and 7.1 mm obtained by EBSD. When IE=0 mm, the sample forms a ring-shaped non-basal texture. When IE=4.1 mm, it is still a non-basal texture, but basal texture components

appear. This may be related to extensive activation of the basal slip system. When the deformation is further increased to IE=7.1 mm, a strong basal texture is formed. As discussed above, {10 12} extension twinning is initiated in a large number at this stage, and {10 12} extension twinning is an important reason for the formation of basal texture [22–24]. Therefore, the reasons why basal texture components increase continuously are that the basal slip at the early stage of deformation and {10 12} extension twinning are activated continuously.

Basal slip is the most easily activated dislocation system in magnesium alloys at room temperature [25]. According to Schmid law, the difficulty of activating the slip system can be measured by the Schmid factor (SF). Therefore, the SF for basal slip is calculated. Considering that the

sheet is subjected to the force from all directions of the punch during the Erichsen cupping test, the force is simplified to the force along the three directions of RD, TD and ND.

The SFs of the basal slip for the cupped samples with IE=0 mm and 4.1 mm in three directions were calculated, as shown in Fig. 11. It can be seen that there are two obvious changes in the average SF of the basal slip system in different directions from IE=0 mm to IE=4.1 mm. In the RD, the average value decreases from 0.32 to 0.28, but it increases from 0.31 to 0.35 in the TD, indicating that in the early deformation period, the basal slip system starts in the TD more easily when the sheet is subjected to complex stress. This may be related to the non-basal texture of the annealed GZ31 sheet with a texture peak towards TD. A similar phenomenon [26] was also found in an AZ31 sheet

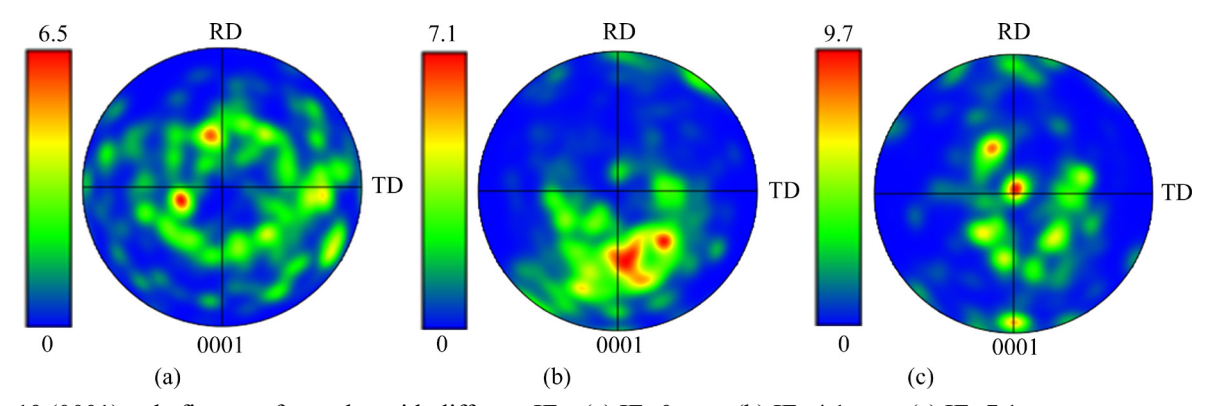


Fig. 10 (0001) pole figures of samples with different IEs: (a) IE=0 mm; (b) IE=4.1 mm; (c) IE=7.1 mm

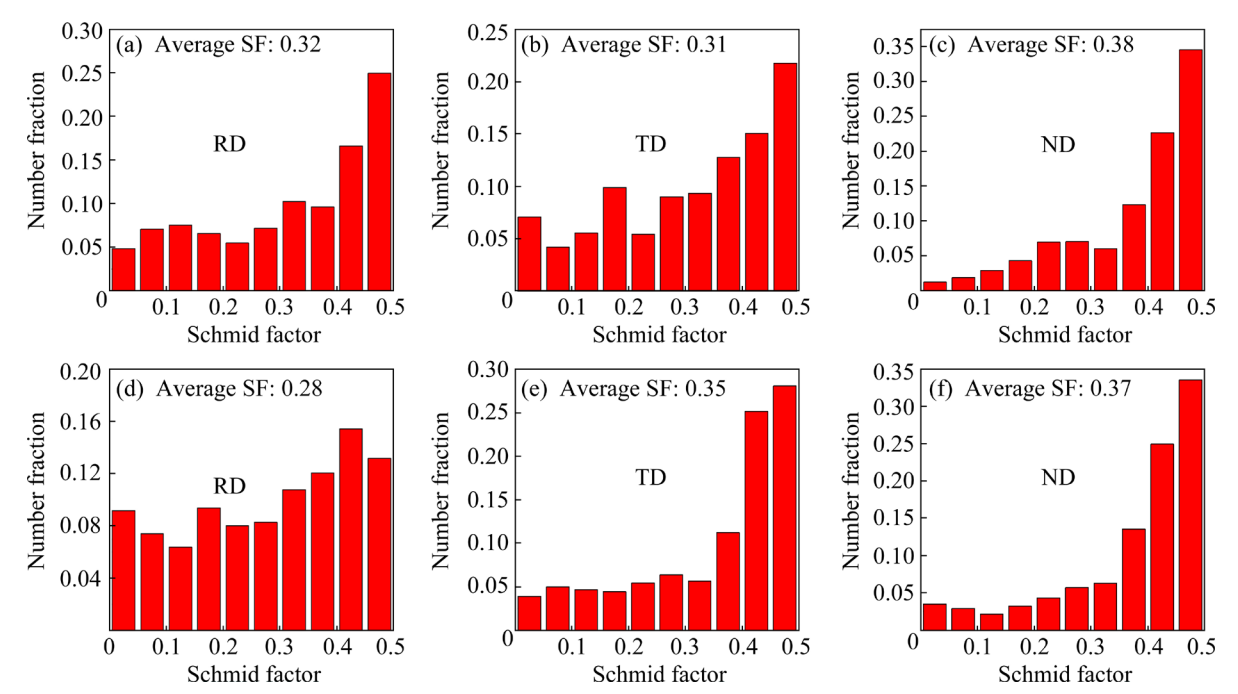


Fig. 11 SF distribution of basal slip system with different IEs in different stress directions: (a-c) IE=0 mm; (d-f) IE=4.1 mm

with a special separated double-peak non-basal texture when the sheet was stretched along the direction of separation.

The slip system initiated at different stages may be different during the Erichsen cupping test. To confirm the type of dislocation slip, the SF distribution of the basal slip, prismatic slip and pyramidal slip systems of the samples with IE=4.1 mm and 7.1 mm along the TD (because of the TD-split texture) was analyzed, as shown in Fig. 12.

When IE=4.1 mm, the average SFs of basal

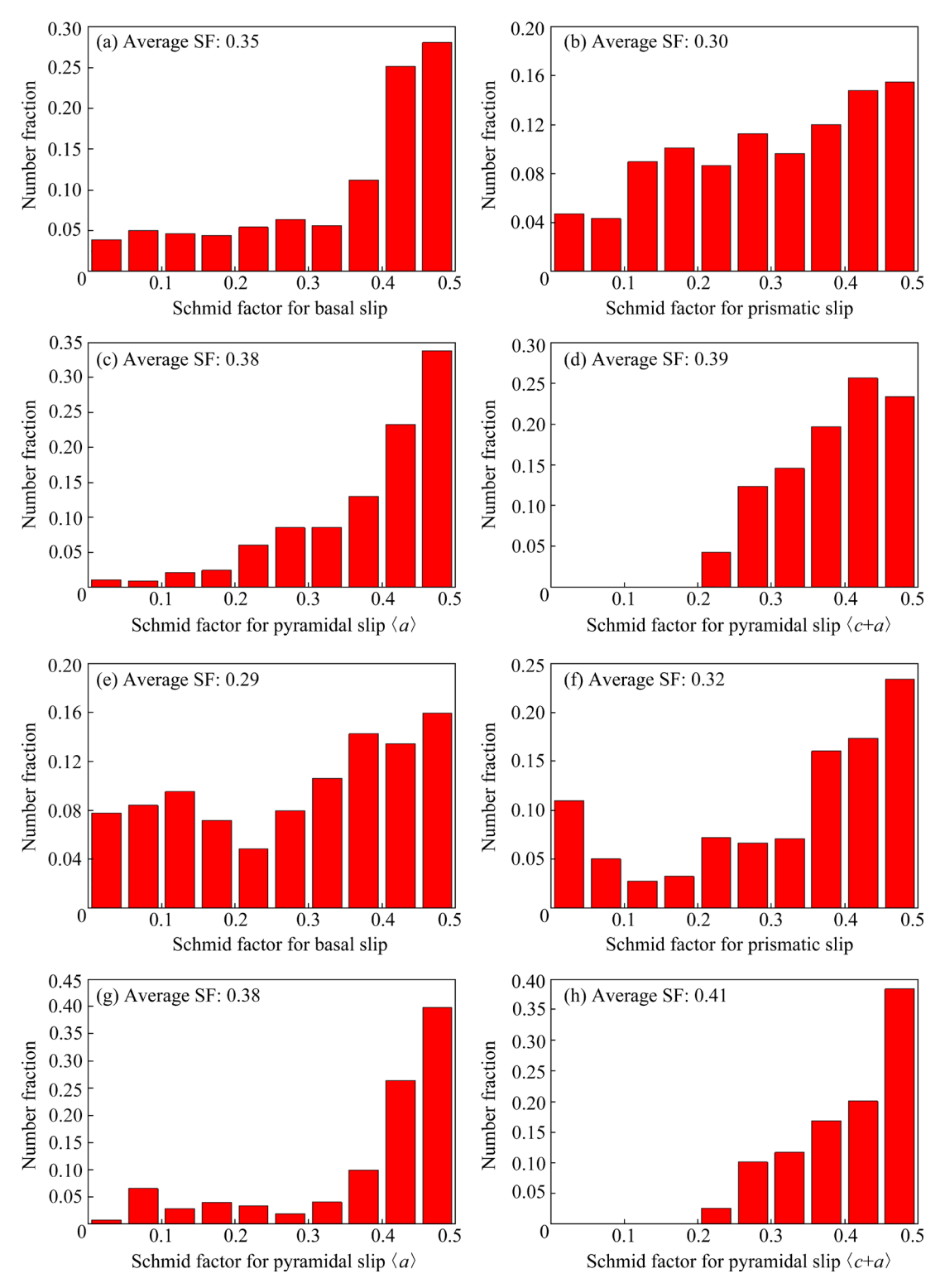


Fig. 12 SF distribution of different slip systems along TD of samples with different IEs: (a-d) IE=4.1 mm; (e-h) IE=7.1 mm

slip, prismatic slip, pyramidal $\langle a \rangle$ and pyramidal $\langle c+a\rangle$ slip systems are 0.35, 0.30, 0.38 and 0.39, respectively, showing that the basal slip and the pyramidal slip systems are more active than the prismatic slip system. When IE=7.1 mm, the average SFs of basal slip, prismatic slip, pyramidal $\langle a \rangle$ slip and pyramidal $\langle c+a \rangle$ slip systems are 0.29, 0.32, 0.38 and 0.41, respectively, indicating that the pyramidal slip systems are more active than the basal slip and prismatic slip systems. From IE=4.1 mm to IE=7.1 mm, the average SFs of the basal slip system decrease from 0.35 to 0.29, while the average SFs of the prismatic slip system and the pyramidal slip system have no significant change. It is inferred that the basal slip system and the pyramidal slip system dominate the deformation at the beginning, and then the pyramidal slip system becomes more active as the deformation increases.

Twinning is the main deformation mode to coordinate the c-axis of grains in magnesium alloy. {10 12} extension twinning has the smallest critical shear variable and lower CRSS, so it is most likely to occur. NAVE and BARNETT et al [27] confirmed by simulation and experimental observation that {1012} extension twinning can improve the uniform elongation of magnesium alloys, while compression twinning and second twinning can easily lead to the generation of microcracks, thus reducing the uniform elongation. A large number of {1012} extension twins also appear during the Erichsen cupping test in this study. Therefore, the nucleation and evolution of extension twinning during the Erichsen cupping test were analyzed.

Figures 13(a) and (b) show IPF maps containing twin grains with IE=4.1 mm and 7.1 mm, respectively. With the increase in IE, the number and the volume fraction of twins within a single grain increase significantly, as twin variants occur. Figures 14 and 15 show the EBSD analysis results of a single typical grain containing twins selected from Figs. 13(a) and (b), respectively, where M and T represent the matrix of the grain and twin bands, respectively. It can be seen from Fig. 14(a) that when IE=4.1 mm, the twin has grown significantly to swallow the parent grain, but has not yet produced other {1012} twinning variants at this time (Fig. 14(c)). When IE=7.1 mm, as shown in Fig. 15(a), multi-extension twins are activated in the grain. In Fig. 15(b), it can be observed that the

angular relationship between two activated twin variants T_1 and T_2 is approximately 61°, which is consistent with the special boundary 60.4° $\{10\overline{12}\} - \{10\overline{12}\}\langle10\overline{10}\rangle$ [28], indicating that T_1 and T_2 are from different twin variant pairs. T_1 and T_2 are in ortho-position (Fig. 15(e)). Similar analysis has also been done for twin variants T_1 and T_3 , as shown in Fig. 15(c), in which the angular relationship (60.0°) between T_1 and T_3 matches the special grain boundary 60.0° $\{10\overline{12}\} - \{10\overline{12}\}\langle10\overline{10}\rangle$, meaning that T_1 and T_3 are in the meta-position (Fig. 15(e)).

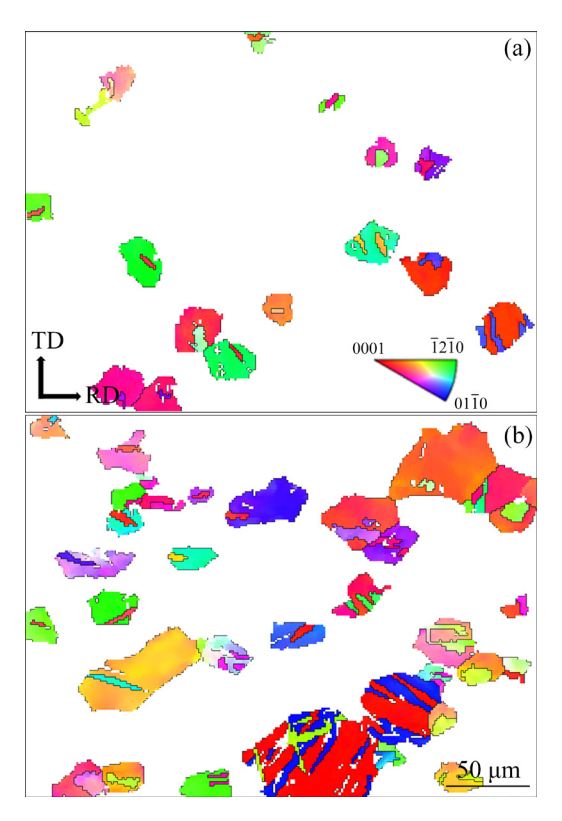


Fig. 13 IPF maps containing only twin grains: (a) IE= 4.1 mm; (b) IE=7.1 mm

SINGH et al [29] studied the Erichsen cupping test of Mg–Al alloys, and the results show that: for basal-textured sheets, as the IE increases, the number of the twins gradually increases firstly and then gradually decreases, showing a "de-twinning" phenomenon; the plastic deformation activated by the basal slip and pyramidal $\langle c+a \rangle$ slip is the main deformation mode, but there is only basal slip and the pyramidal $\langle c+a \rangle$ slip can be ignored when IE>0.5 mm.

However, the behaviors of dislocation slip and twinning are quite different in the present sheet with non-basal texture. During the process of deformation with IE from 0 to 4.1 mm, basal slip

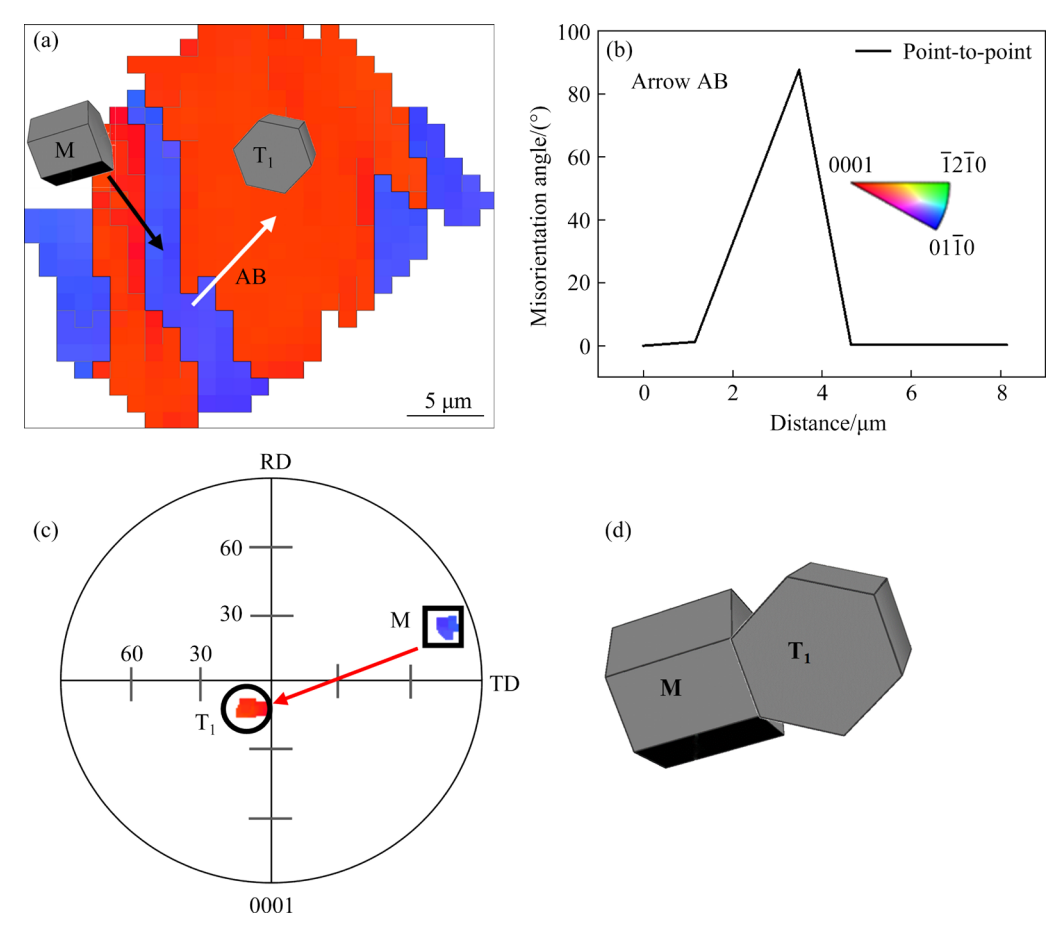


Fig. 14 Twinning morphology (a) of single typical grain selected from Fig. 13(a), line profile (b) of misorientation angle along white arrow AB in Fig. 14(a), orientation of parent matrix (black square) and $\{10\overline{12}\}$ twinning variants (black triangles or circles) in $\{0001\}$ pole figure (c), and three-dimensional crystallographic relationship between parent grain (M) and selected variants (T₁) (d)

and pyramidal $\langle c+a \rangle$ slip are the main deformation mechanisms, and $\{10\overline{12}\}$ extension twinning is a supplement. At the stage of the Erichsen cupping test, when IE changes from 4.1 to 7.1 mm, pyramidal $\langle c+a \rangle$ slip and twinning are the main deformation modes, and basal slip is the secondary deformation mode. The $\{10\overline{12}\}$ extension twinning gradually becomes active to accommodate the deformation, and no de-twinning is observed during the whole process.

The IE of the Mg-Al sheet with a basal texture is approximately 4.5 mm, while that of GZ31 sheet with a non-basal texture can reach 7.3 mm. By comparing the cupping deformation mechanism, it can be found that more non-basal slip systems and the nucleation and growth of {1012} extension twins are more beneficial to obtaining higher IE during the deformation process. In addition to the effect of non-basal texture on the plastic deformation mechanism, rare earth elements can

reduce the CRSS of non-basal slip, making non-basal slip more active, and benefits the high formability.

3.4 Fracture mechanism

When the IE is 7.3 mm, the cupped sample has cracks at the edge of the ring where the punch contacts the sheet. With the gradual increase in strain, micro-cracks appear and finally lead to sheet fracture. The micro-cracks are generated from the middle of the cupped sample, then propagate and extend to both ends along the approximately parallel TD, and gradually, branch as the crack continues to expand, with a mixed fracture mode of transgranular and intergranular fracture, as shown in Fig. 16.

Studies [30] have shown that the AZ31 hotrolled sheet has a strong basal texture with a wider distribution in the RD, and the elongation along the RD is higher than that in the TD. Thus, the cracks

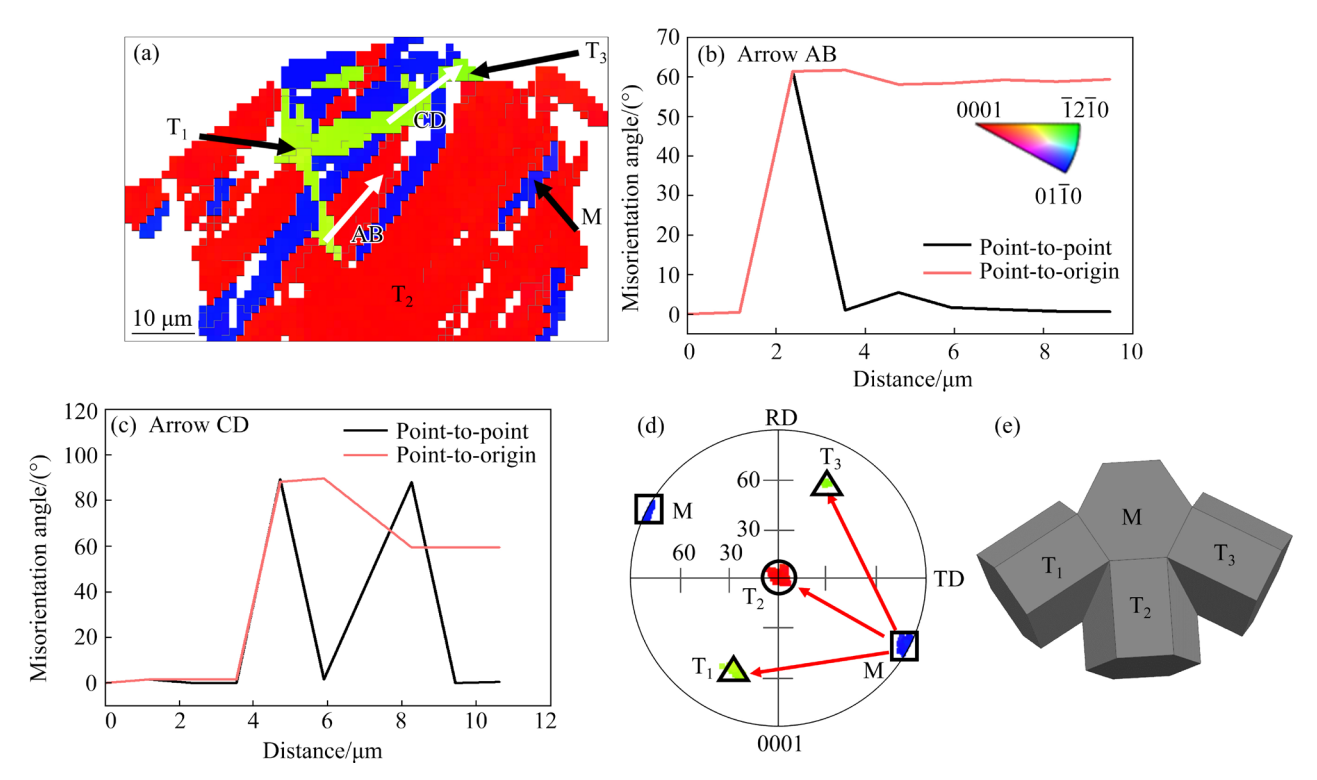


Fig. 15 Twinning morphology (a) of single typical grain selected from Fig. 13(b), line profile (b) of misorientation angle along white arrow AB in Fig. 15(a), line profile (c) of misorientation angle along white arrow CD in Fig. 15(a), orientation of parent matrix (black square) and {10 12} twinning variants (black triangles or circles) in {0001} pole figure (d), and three-dimensional crystallographic relationship between parent grain (M) and selected variants (T₁, T₂ and T₃) (e)

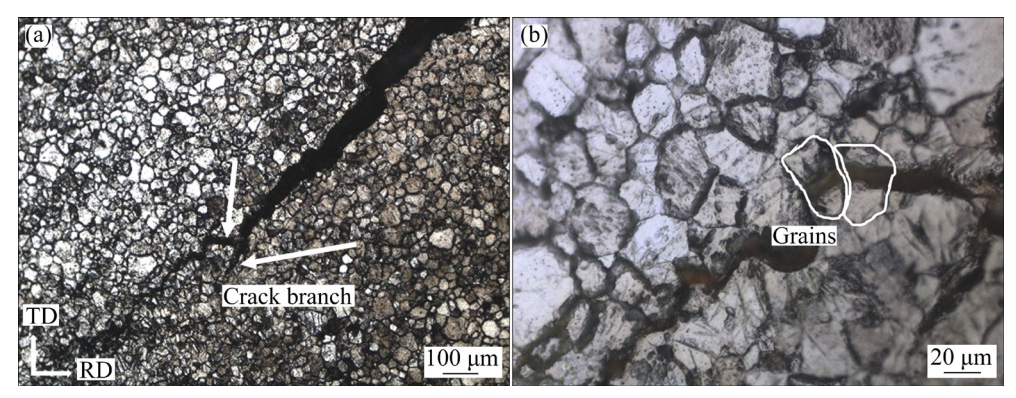


Fig. 16 Microstructure of cupped sample with IE=7.3 mm: (a) Lower magnification; (b) Higher magnification

are generated and propagate mostly parallel to the RD during the Erichsen cupping test. In contrast, the texture of the GZ31 sheet is more tilting to TD, and the elongation in the TD was higher. A similar phenomenon also appears in hot-rolled Mg–Zn–Y alloy sheets [31]. The texture type affects the plastic deformation and the mechanical properties in all directions, as well as the macroscopic fracture behavior. Because the Erichsen cupping test is circumferentially symmetrical and bears the same strain in the radial direction, the sheet will crack

along the direction perpendicular to the direction with low plasticity. This is why in the cupping test, the cracks of the AZ31 sheet are perpendicular to the TD, while the cracks of the Mg–Zn–RE sheet are perpendicular to the RD.

To explain the nucleation and evolution of micro-cracks during the Erichsen cupping test, SEM and kernel average misorientation (KAM) images of samples with different IEs were analyzed, as shown in Fig. 17. When IE=0 mm, many second-phase particles could be seen, especially at

grain boundaries (Fig. 17(a)). When IE=4.1 mm, a small number of voids with a diameter of $1-2 \mu m$ can be clearly seen in Fig. 17(b) and Fig. 17(d), occurring near the grain boundaries where many second-phase particles exist. When IE=7.1 mm, some voids have been coalesced to form micro-

cracks at the grain boundaries (Figs. 17(c, e)).

Figure 18 shows the misorientation angle across the cracks of the cupped samples with IE=7.3 mm. The misorientation angle along arrow AB is less than 15°, indicating that the crack is formed along LAGBs. The misorientation angle

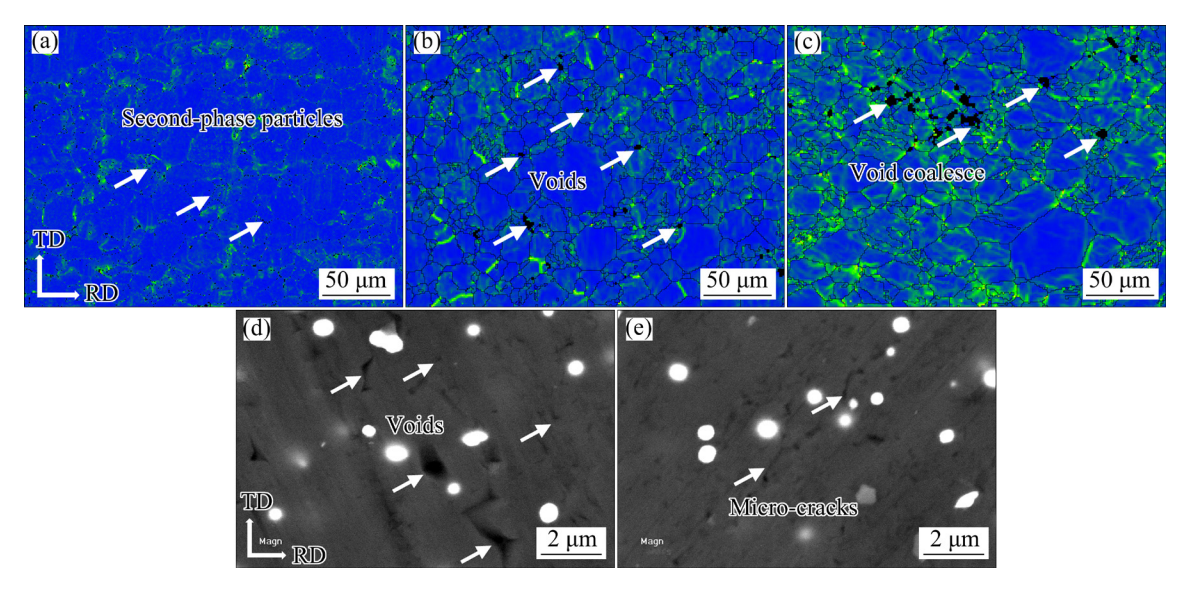


Fig. 17 Micro-crack analysis results of cupped samples: (a-c) KAM maps of samples with IE=0, 4.1 and 7.1 mm, respectively; (d, e) SEM images of samples with IE=4.1 and 7.1 mm, respectively

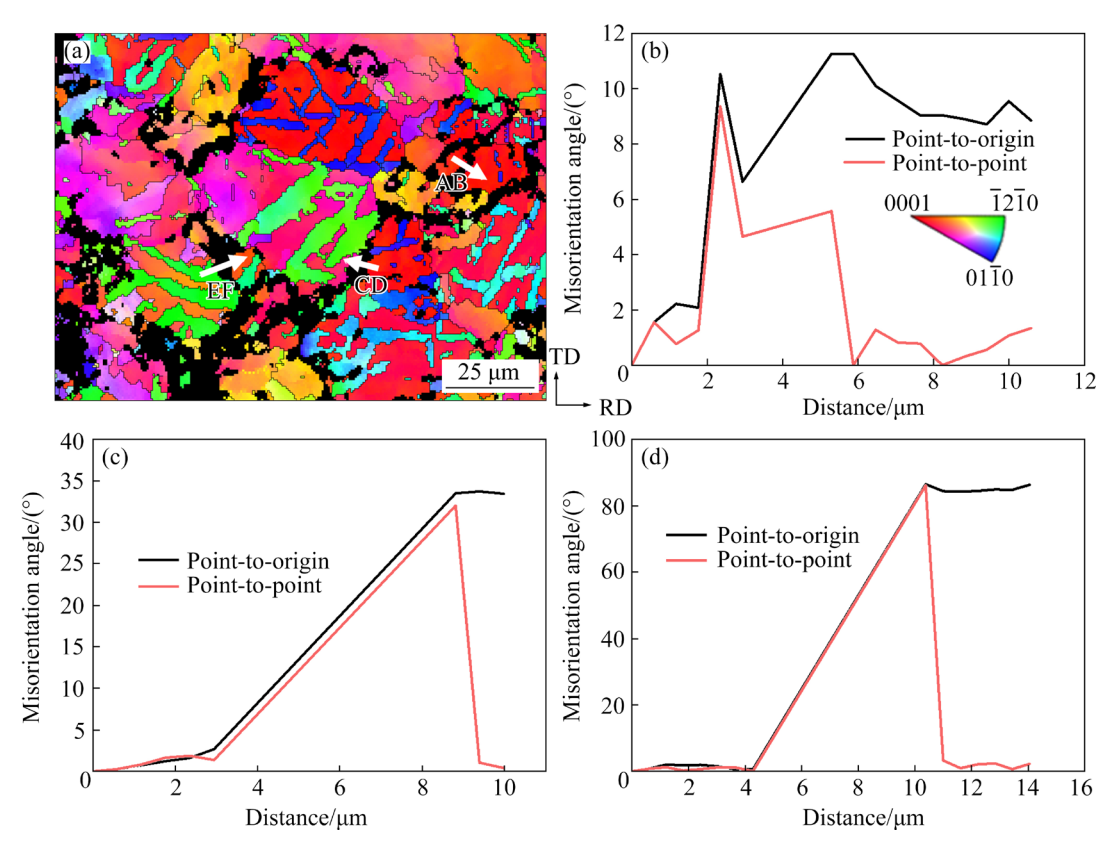


Fig. 18 Misorientation analysis around cracks of sample with IE=7.3 mm: (a) IPF map; (b) Misorientation angle along arrow AB; (c) Misorientation angle along arrow CD; (d) Misorientation angle along arrow EF

along arrow CD is approximately 30°, which is a large-angle grain boundary, indicating that the crack formed at the grain boundaries. The is misorientation angle along arrow is approximately 86°, indicating that cracks are formed at the twin boundaries. According to the statistics in Fig. 18(a), most cracks are formed at the grain boundaries, and few micro-cracks are generated in the intracrystalline and at the twin boundaries.

Based on these, the analysis results should be that when the sheet is deformed, a large number of dislocation slips are hindered by the grain boundaries and the second phase particles at the grain boundaries [32]. Then, the dislocations pile up and entangle with each other, causing stress concentration at the grain boundaries, thus resulting in the formation of voids. The voids coalesce to form small cracks under the further stain, and finally cause the cupped sample to break through.

The main reason for the excellent formability of the Mg-Zn-RE sheet is non-basal texture. The non-basal texture can promote massive {1012} extension twins and basal dislocation slip while inhibiting the initiation of compression twins and secondary twins, which easily become the source of cracks [33]. According to Fig. 7, there are almost no compression twins and secondary twins in the cupped sample of the GZ31 sheet, but a large number of {1012} extension twins. Continuous coarsening of {1012} extension twins inhibits the generation of cracks or dulls the crack tip, improving the continuity of magnesium alloy deformation and enhancing its formability. After the Erichsen cupping test of the AZ31 sheet, many compression twins and secondary twins can be seen [34]. In summary, there were a large number of {10 12} extension twins and no compression twins or secondary twins during the Erichsen cupping test, which is also an important reason why the cupping performance of the Mg-Zn-RE sheet is better than that of AZ31 at room temperature.

4 Conclusions

(1) The annealed GZ31 sheet has a relatively uniform microstructure with an average grain size of $39.32 \, \mu m$, and exhibits a typical non-basal texture with two TD-split components. Even if the

- grain size is relatively large, the IE at room temperature still reaches 7.3 mm, which is much higher than that of the AZ31 sheet.
- (2) With IE from 0 to 4.1 mm, the basal slip and pyramidal $\langle c+a \rangle$ slip first start to play a leading role, and $\{10\,12\}$ extension twinning is a supplement. At the stage of IE from 4.1 to 7.1 mm, pyramidal $\langle c+a \rangle$ slip and extension twinning are the main deformation modes, and basal slip is the secondary deformation mode.
- (3) A large amount of dislocation movement is hindered by grain boundaries and second phase particles, and then dislocations pile up and entangle with each other to form voids. The voids expand and gather to form micro-cracks, and further expand together to cause the cupped sample to fail.
- (4) The GZ31 sheet shows high IE at room temperature because the weak non-basal texture and rare_earth element are favorable for basal slip, {1012} extension twining and pyramidal slip to coordinate deformation. Therefore, compression twinning, secondary twinning and shear deformation which can easily lead to cracks, can be avoided.

Acknowledgments

This work was financially supported by the Natural Science Foundation of Liaoning Province, China (No. 2020-MS-004), the National Natural Science Foundation of China (Nos. 51601193, 51701218), the National Key Research and Development Program of China (No. 2016YFB0301104), the State Key Program of National Natural Science of China (No. 51531002), and the Natural Science Foundation of Shandong Province, China (No. ZR2021ME241).

References

- [1] CHE Bo, LU Li-wei, WU Zhi-qiang, ZHANG Hua, MA Min, LUO Jun, ZHAO Hong-mei. Dynamic recrystallization behavior and microstructure evolution of a new Mg-6Zn-1Gd-1Er alloy with and without pre-aging treatment [J]. Materials Characterization, 2021, 181: 1-15.
- [2] BAZHENOV V E, SAIDOV S S, TSELOVALNIK Y V, VOROPAEVA O O, PLISETSKAYA I V, TOKAR A A, BAZLOV A I, BAUTIN V A, KOMISSAROV A A, KOLTYGIN A V, BELOV V D. Comparison of castability, mechanical, and corrosion properties of Mg-Zn-Y-Zr alloys containing LPSO and W phases [J]. Transactions of Nonferrous Metals Society of China, 2021, 31: 1276-1290.
- [3] SONG Jiang-feng, SHE Jia, CHEN Dao-lun, PAN Fu-sheng. Latest research advances on magnesium and magnesium

- alloys worldwide [J]. Journal of Magnesium and Alloys, 2020, 8: 1-41.
- [4] TAYLOR S, WEST G D, MOGIRE E, TANG F, KOTADIA H R. Superplastic forming characteristics of AZ41 magnesium alloy [J]. Transactions of Nonferrous Metals Society of China, 2021, 31: 648-654.
- [5] YANG Yan, XIONG Xiao-ming, CHEN Jing, PENG Xiao-dong, CHEN Dao-lun, PAN Fu-sheng. Research advances in magnesium and magnesium alloys worldwide in 2020 [J]. Journal of Magnesium and Alloys, 2021, 9: 705–747.
- [6] CHUN Y B, DAVIES C H J. Investigation of prism ⟨a⟩ slip in warm-rolled AZ31 alloy [J]. Metallurgical and Materials Transactions A, 2011, 42: 4113–4125.
- [7] HU Hong-jun, HONG Xing, TIAN Ye, ZHANG Ding-fei. AZ31 magnesium alloy tube manufactured by composite forming technology including extruded-shear and bending based on finite element numerical simulation and experiments [J]. The International Journal of Advanced Manufacturing Technology, 2021, 115: 2395–2402.
- [8] JEONG H T, HA T K. Texture development in a warm rolled AZ31 magnesium alloy [J]. Journal of Materials Processing Technology, 2007, 187: 559–561.
- [9] HU Hong-jun, ZHANG Ding-fei, YANG Ming-bo, DENG Ming. Grain refinement in AZ31 magnesium alloy rod fabricated by extrusion-shearing severe plastic deformation process [J]. Transactions of Nonferrous Metals Society of China, 2011, 21: 243–249.
- [10] YAN Hong, SHAO Xiao-hong, LI Hui-ping, CHEN Rong-shi, CUI Hong-zhi, HAN En-hou. Synergization of ductility and yield strength in a dilute quaternary Mg–Zn–Gd–Ca alloy through texture modification and Guinier–Preston zone [J]. Scripta Materialia, 2022, 207: 1–6.
- [11] AGNEW S R, DUYGULU Ö. Plastic anisotropy and the role of non-basal slip in magnesium alloy AZ31B [J]. International Journal of Plasticity, 2005, 21: 1161–1193.
- [12] HAN Ting-zhuang, HUANG Guang-sheng, WANG You-gen, WANG Guan-gang, ZHAO Yan-chun, PAN Fu-sheng. Microstructure and formability evolutions of AZ31 magnesium alloy sheets undergoing continuous bending process [J]. Transactions of Nonferrous Metals Society of China, 2016, 26: 2043–2050.
- [13] ZHAO Yan-chun, ZHANG Hua, FAN Jian-feng, WANG Li-fei, ZHANG Qiang, PENG Cheng, DONG Hong-biao, XU Bing-she. Grain refining and improving mechanical properties of AZ31 Mg alloy sheets by multi-pass warm rolling with falling temperature [J]. Journal of Materials Research, 2018, 33: 2827–2834.
- [14] CHINO Y, SASSA K, MABUCHI M. Texture and stretch formability of Mg-1.5mass%Zn-0.2mass%Ce alloy rolled at different rolling temperatures [J]. Materials Transactions, 2008, 49: 2916-2918.
- [15] WU Yi-ping, XIONG Han-qing, JIA Yu-zhen, XIE Shao-hui, LI Guo-feng. Microstructure, texture and mechanical properties of Mg-8Gd-4Y-1Nd-0.5Zr alloy prepared by pre-deformation annealing, hot compression and ageing [J]. Transactions of Nonferrous Metals Society of China, 2019, 29: 976-983.
- [16] YAN Hong, CHEN Rong-shi, HAN En-hou. Room-

- temperature ductility and anisotropy of two rolled Mg–Zn–Gd alloys [J]. Materials Science and Engineering: A, 2010, 527: 3317–3322.
- [17] CAI Zheng-xu, JIANG Hai-tao, TANG Di, MA Zhao, KANG Qiang. Texture and stretch formability of rolled Mg-Zn-RE(Y, Ce, and Gd) alloys at room temperature [J]. Rare Metals, 2013, 32: 441-447.
- [18] KAMIKAWA N, MORINO H. Quantitative analysis of load-displacement curves in Erichsen cupping test for low carbon steel sheet [J]. Metallurgical and Materials Transactions A, 2019, 50: 5023-5037.
- [19] HOSEINI-ATHAR M M, MAHMUDI R. Effect of Zn content on hot deformation behavior of extruded Mg-Gd-Zn alloys [J]. Materials Science and Engineering: A, 2019, 759: 745-753.
- [20] HUANG Xin-sheng, SUZUKI K, CHINO Y, MABUCHI M. Influence of initial texture on cold deep drawability of Mg-3Al-1Zn alloy sheets [J]. Materials Science and Engineering: A, 2013, 565: 359-372.
- [21] XIN Yun-chang, WANG Mao-yin, ZENG Zhen, HUANG Guang-jie, LIU Qing. Tailoring the texture of magnesium alloy by twinning deformation to improve the rolling capability [J]. Scripta Materialia, 2011, 64: 986–989.
- [22] JIANG Ming-guang, XU Chao, YAN Hong, FAN Guo-hua, NAKATA T, LAO Chang-shi, CHEN Rong-shi, KAMADO S, HAN En-hou, LU Bing-heng. Unveiling the formation of basal texture variations based on twinning and dynamic recrystallization in AZ31 magnesium alloy during extrusion [J]. Acta Materialia. 2018, 157: 53-71.
- [23] ZHAO Y R, CHANG L L, GUO J, JIN Y P. Twinning behavior of hot extruded AZ31 hexagonal prisms during uniaxial compression [J]. Journal of Magnesium and Alloys, 2019, 7: 90–97.
- [24] ZENG Zhuo-ran, BIAN Ming-zhe, XU Shi-wei, DAVIES C H J, BIRBILIS N, NIE Jian-feng. Texture evolution during cold rolling of dilute Mg alloys [J]. Scripta Materialia, 2015, 108: 6–10.
- [25] CHAPUIS A, DRIVER J H. Temperature dependency of slip and twinning in plane strain compressed magnesium single crystals [J]. Acta Materialia, 2011, 59: 1986–1994.
- [26] CHEN Yu, HU Li, SHI Lai-xin, ZHAO Tao, TU Jian, CHEN Qiang, YANG Ming-bo. Effect of texture types on microstructure evolution and mechanical properties of AZ31 magnesium alloy undergoing uniaxial tension deformation at room temperature [J]. Materials Science and Engineering: A, 2020, 769: 1–9.
- [27] NAVE M D, BARNETT M R. Microstructures and textures of pure magnesium deformed in plane-strain compression [J]. Scripta Materialia, 2004, 51: 881–885.
- [28] PEI Y, GODFREY A, JIANG J, ZHANG Y B, LIU W, LIU Q. Extension twin variant selection during uniaxial compression of a magnesium alloy [J]. Materials Science and Engineering A, 2012, 550: 138–145.
- [29] SINGH M, CHOUBEY A K, SASIKUMAR C. Formability analysis of aluminium alloy by Erichsen cupping test method [J]. Materials Today: Proceedings, 2017, 4: 805–810.
- [30] CHINO Y, SASSA K, KAMITA A, MABUCHI M. Influence of rolling routes on press formability of a rolled AZ31 Mg alloy sheet [J]. Materials Transactions, 2006, 47: 2555–2560.

- [31] CHINO Y, SASSA K, MABUCHI M. Texture and stretch formability of a rolled Mg–Zn alloy containing dilute content of Y [J]. Materials Science and Engineering: A, 2009, 513/514: 394–400.
- [32] FEKETE K H, DROZDENKO D, CAPEK J, MATHIS K, TOLNAI D, STARK A, GARCES G, DOBRON P. Hot deformation of Mg-Y-Zn alloy with a low content of the LPSO phase studied by in-situ synchrotron radiation diffraction [J]. Journal of Magnesium and Alloys, 2020, 8:
- 199–209.
- [33] ZHOU Na, ZHANG Zhen-yan, JIN Li, DONG Jie, CHEN Bin, DING Wen-jiang. Ductility improvement by twinning and twin-slip interaction in a Mg-Y alloy [J]. Materials & Design, 2014, 56: 966–974.
- [34] NAZARI-ONLAGHI S, SADEGHI A, KARIMPOUR M, PEKGULERYUZ M. Fracture micro-mechanisms in hot-rolled AZ31 and AZ31-Sr magnesium alloys [J]. Materials Science and Engineering: A, 2021, 812: 141107.

Mg-Zn-Gd 板材在 Erichsen 杯突试验过程中的 组织演变和变形机理

陈 勇 ^{1,2}, 闫 宏 ^{1,3}, 王 丹 ⁴, 陈荣石 ^{1,2}

- 1. 中国科学院 金属研究所 师昌绪先进材料创新中心, 沈阳 110016;
 - 2. 中国科学技术大学 材料科学与工程学院, 沈阳 110016;
 - 3. 山东科技大学 材料科学与工程学院, 青岛 266590;
 - 4. 中国航发沈阳黎明航空发动机有限责任公司, 沈阳 110043

摘 要:对 GZ31 板材在室温和不同压下量条件下进行 Erichsen 杯突试验,获得 4 个杯突值分别为 2.0、4.1、7.1 和 7.3 mm 的样品。利用 OM、SEM 和 EBSD 技术手段研究杯突试验时样品的变形机理和断裂机理。结果表明,非基面织构的 GZ31 轧制板材杯突值可达 7.3 mm。在杯突过程中,基面、锥面滑移以及 {10 12} 拉伸孪生是主要的变形方式。位错滑移受到第二相颗粒以及晶界阻碍,相互缠结形成微孔,最后导致材料的断裂。GZ31 板材杯突值高是因为弱的非基面织构以及稀土元素有利于位错滑移和拉伸孪生去协调变形。

关键词: 镁合金; Erichsen 杯突试验; 位错滑移; 孪生

(Edited by Wei-ping CHEN)